LIGHT TRAPPING IN THIN FILM PLASMONIC SOLAR CELLS

V. E. Ferry[1,2], M. A. Verschuuren, H. B. T. Li[4], E. Verhagen[1], R. J. Walters[1],
R. E. I. Schropp[4], H. A. Atwater[2], A. Polman[1]
[1]FOM Institute AMOLF, Science Park 104, 1098 XG Amsterdam, The Netherlands
[2]California Institute of Technology, 1200 E California Blvd., Pasadena CA 91125 USA
[3]Philips Research, High Tech Campus 4, 5656 AE Eindhoven, The Netherlands
[4]Utrecht University, PO Box 80.000, 3508 TA Utrecht, The Netherlands
Tel: +31-20-7547100, Fax: +31 20 7547290, Email: polman@amolf.nl

ABSTRACT: Advanced light management in thin-film solar cells is becoming increasingly important to reduce semiconductor layer thicknesses (and thus costs) while still absorbing the full solar spectrum in the cell. Here, we discuss how the excitation of surface plasmon resonances in metal nanoparticles can serve to enhance the trapping of light in thin-film solar cells. We discuss three geometries, with particles either at the top or back of the cell, or embedded in the solar cell, and compare these different designs. We demonstrate the effectiveness of the plasmonic light trapping concept by presenting experimental data on ultra-thin n-i-p a-Si:H solar cells with plasmonic back reflectors. We show that using a properly designed scattering structure, the performance of cells on randomly textured Asahi substrates can be surpassed. The periodic patterns are made via an inexpensive and scalable nanoimprint method. Electromagnetic modeling is shown to agree well with measurements, and used to understand further details of the device.
Keywords: Light Trapping, Plasmonics, a-Si:H, Optical Properties

1 INTRODUCTION

Photovoltaics have the potential to make a significant contribution to solving the energy problem that our society faces in the next generation. To make power from photovoltaics competitive with fossil fuel technologies, the cost needs to be reduced by a factor of 2-5. Currently a large fraction of the solar cell market is based on crystalline silicon wafers with a thickness of 180-300 μm, and a major fraction of the cell price is due to Si materials and processing costs. Because of this, there is great interest in thin-film solar cells, with film thicknesses in the range 1-2 μm, that can be deposited on cheap module-sized substrates such as glass, plastic or stainless steel. Thin-film solar cells are made from a variety of semiconductors including amorphous and polycrystalline Si, GaAs, CdTe, and $CuInSe_2$, as well as organic semiconductors. A major limitation in all thin-film solar cell technologies is that the absorbance of near-bandgap light is small, in particular for the indirect bandgap semiconductor silicon. Therefore, structuring the thin-film solar cell so that light is trapped inside in order to increase the absorbance ("light trapping") is very important. A significant reduction in thin-film solar cell thickness would also enable the large-scale use of scarce semiconductor materials that are only available in the earth's crust in limited quantities, such as In and Te.

2 PLASMONIC DESIGN

Light trapping in thin-film solar cells can be achieved using suitably engineered metal nanostructures integrated in the thin-film solar cell designs. Three light trapping geometries are indicated schematically in Fig. 1 [1]. All designs use the controlled scattering and/or optical near field enhancement due to the excitation of surface plasmons (resonant excitations of free electrons) in metal nanoparticles to enhance the absorption of light in a thin-film solar cell.

Nanoparticles made on the surface of a solar cell (Fig. 1(a)) act as efficient scatterers of light, causing a

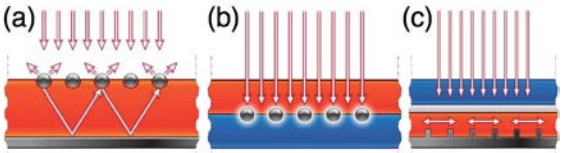

Figure 1: Plasmonic light trapping geometries for thin-film solar cells. (a) Light trapping by scattering from metal nanoparticles at the surface of the solar cell. Light is preferentially scattered and trapped into the semiconductor thin film by multiple and high-angle scattering, causing an enhancement of the effective optical path length in the cell. (b) Light trapping by the excitation of localized surface plasmons in metal nanoparticles embedded in the semiconductor. The excited particle's near field causes the creation of electron-hole pairs in the semiconductor. (c) Light trapping by the excitation of surface plasmon polaritons at the metal-semiconductor interface. A corrugated metal back surface couples light to surface plasmon polariton or photonic modes that propagate in the plane of the semiconductor layer.

redistribution of light in the solar cell and thus an enhancement of the effective path length [2]. Such particle arrays can provide near-perfect impedance matching between incident light and the Si active layer over a broad spectral range. Light can make multiple passes inside the film by repeated scattering from the particles at the surface. This geometry is particularly interesting for thin-film solar cell materials that cannot be combined with a textured backreflector, such as multicrystalline Si that is difficult to conformally grow onto a corrugated surface. Also, applying metal nanoparticle arrays on top of a flat surface, rather than texturing the surface itself, is advantageous as the latter causes unwanted additional surface recombination. The metal can be electrically isolated from the semiconductor using a thin dielectric spacer layer [3]. The scattering cross section of plasmonic particles can be as high as 10 times the geometrical cross section, so that a surface coverage of order 10% is sufficient to reach full interaction with the incident light [4]. These scattering

cross sections are spectrally dependent, and their resonance wavelength can be tuned through modification of the shape, size, noble metal choice, and surrounding material.

Embedding metal nanoparticles inside the active layer of the solar cell (Fig. 1(b)) is of interest for materials that show poor carrier diffusion. In this case, the cell must be made thin in order to be able collect all carriers, which comes at the expense of reduced optical absorption. The embedded metal nanoparticles then serve as optical antennas that strongly interact with the incoming light. The optical near-field around the antennas (with an extent of several tens of nms about the particle) then couples to the semiconductor. This approach is limited by Ohmic damping in the metal, and thus works best if absorption in the semiconductor is very strong. Some organic or direct-bandgap semiconductors may benefit from this approach [5]. The metal nanoparticles in the design of Fig. 1(a) must be relatively large so that they are strong scatterers rather than absorbers (absorption scales with volume, scattering with volume squared), but in the design of Fig. 1(b), scattering is unwanted and small particles (10-20 nm in diameter) are desirable. At such small size, these particles can indeed be integrated with thin semiconductor layers. Obviously such an approach will only work it the incorporation of the metal does not deteriorate the electrical characteristics of the semiconductor.

In the third design (Fig. 1(c)), metallic nanostructures are integrated with the metallic backcontact of the solar cell and serve as strong scatterers that couple light to in-plane waveguide modes of the solar cell. The advantage of this geometry is that the metal nanostructures do not interact with blue and green light as that is directly absorbed as it enters the solar cell, but rather redirect the red light that would otherwise be poorly absorbed. Below, we demonstrate the effectiveness of this approach for amorphous Si thin film solar cells [6-9].

3 CELL FABRICATION

Nanopatterns were made onto glass substrates using substrate conformal imprint lithography (SCIL) [10]. A master silicon wafer was first patterned using electron beam lithography, where the area of the total patterned area was 10 cm by 5 cm, separated into 6 mm by 6 mm squares of distinct patterns. A composite polydimethyl siloxane (PDMS) stamp was molded from the master. The patterns were embossed into 100 nm of silica sol-gel on glass via the sequential evacuation of a system of grooves with 20 millibar pressure. The stamp was then removed via sequential re-pressurization. The sol-gel solidifies at room temperature while the stamp is in place, and is cured at 200°C after stamp removal. The sol-gel is stable to at least 450°C, and non-absorbing. Both the master wafer and the stamp are reusable thousands of times.

The patterns fabricated were square arrays of hemispherical particles, at two pitches (500 and 700 nm) and four diameters (200 – 275 nm) as shown in scanning electron microscopy (SEM) images in Figure 2. The nanostructures have a hemiellipsoidal shape after coating, and they are all 100 nm tall with varying width. Several copies of each of the 8 cells shown in Figure 2 were made on the master substrate, along with flat reference cells, to ensure that all measurements are a result of patterning and not of deposition inhomogeneity.

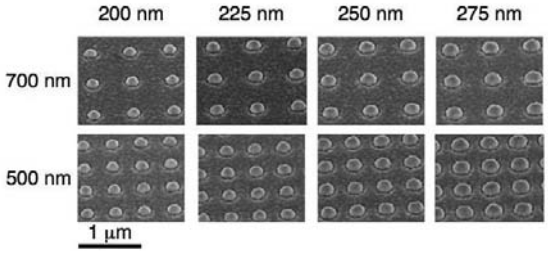

Figure 2: SEM images of nanopatterned Ag back contacts

The patterned silica was then sputter-coated with 200 nm of Ag and 130 nm of ZnO:Al to form a standard back contact. Either 160 nm or 340 nm of a-Si:H (total n-i-p thickness) was deposited by 13.56 MHz plasma enhanced chemical vapor deposition on top of the patterned contacts, and 80 nm thick, 4 mm x 4 mm pads of indium tin oxide (ITO) sputtered as a top contact. The nanopatterns were clearly visible through the ultrathin silicon, so the ITO pads were easily aligned to the bottom contacts. The thickness of the ITO was chosen to also act as an antireflective coating. A metal contact grid was evaporated over the ITO pads.

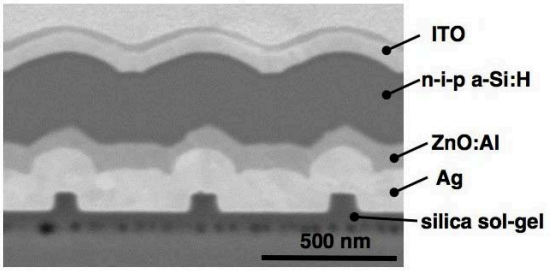

Figure 3: Cross section of cell with 340 nm thick a-Si:H after fabrication showing that the layer depositions are highly conformal.

Several different nanopatterns and reference cells were fabricated during the same deposition run to control for deposition variations. A master substrate was designed containing a variety of nanopatterns as well as flat reference cells, tiled with rotation to account for inhomogeneities. A second substrate of randomly textured Asahi U-type glass was included in the same deposition.

The topography of the resulting cells was investigated using atomic force microscopy (AFM) and focused ion beam (FIB) cross sections. Each deposition was conformal, so that the underlying pattern transferred through every layer, as illustrated in Figure 3. Both the top and back interfaces of the cell thus are therefore nanopatterned, with slightly different diameters due to the conformal coating.

4 ELECTRICAL MEASUREMENTS

Measurements were taken under AM1.5 one sun illumination (100 mW/cm^2), and external quantum efficiency (EQE) measurements were taken using a Xenon lamp source through a monochromator with one sun light bias applied. External quantum efficiency (EQE) measurements were taken at both 0.0 volts and at -

1.0 volt. Angle resolved EQE measurements were taken using a supercontinuum laser in combination with a monochromator.

Cell design	*Thickness (nm)*	*V_{oc} (V)*	*J_{sc} (mA/cm^2)*	*FF*	*Eff. (%)*
Flat	160	0.89	7.9	0.68	4.8
Asahi	160	0.87	10.8	0.64	6.0
500 nm	160	0.89	11.5	0.66	6.6
700 nm	160	0.88	10.4	0.65	5.6
flat	340	0.84	10.5	0.58	5.1
500 nm	340	0.85	13.4	0.56	6.4
700 nm	340	0.84	13	0.56	6.1

Table I: Summary of electrical measurements for measured cells.

Table I shows a summary of the averaged electrical measurements for the 160 nm cells. As expected for devices with varying degrees of light trapping, the main difference between the devices is in J_{sc}. Little difference is observed in JV measurements for different diameters. However, a strong dependence is observed on pitch of the nanostructures. All of the patterned cells show a significant enhancement over the flat reference cell, increasing J_{sc} by 30-50%. Notably, J_{sc} of the 500 nm pitch cells exceeds that of the randomly textured Asahi cells, while the 700 nm pitch cells do not. The highest efficiency was measured, for a cell with 275 nm diameter Ag nanoparticles with a 500 nm pitch, which shows J_{sc} =11.8 mA/cm^2, compared to J_{sc}=10.8 mA/cm^2 for the best Asahi cell. This corresponds to a J_{sc} enhancement of 9.3%.

The open circuit voltages (V_{oc}) and fill factors (FF) are similar for all cells, indicating that a difference in semiconductor quality is not the origin of the difference between the Asahi cells and the nanopatterned cells. We do note that although J_{sc} is smaller in the 160 nm thick cells than in the 340 nm thick cell, the efficiency of the best performing device in the 160 nm case and the 340 nm thick case are nearly identical (6.4/6.6%). This is mainly due to the fact that the thinner cell has a higher V_{oc} which we attribute to decreased bulk recombination due to the reduced thickness.

Figure 4 shows EQE measurements for several cells from the 160 nm thick a-Si:H deposition. The shape of the curves for the nanopatterned and reference cells are highly reproducible across the substrate. On the blue side of the spectrum, from 350 – 550 nm, all four cases are nearly identical. The main difference in the photocurrent is from 550 – 650 nm, where the photocurrent from the 500 nm nanopatterned cell clearly exceeds the photocurrent from the randomly textured Asahi cell. From 650 nm – 800 nm all of the nanopatterned and Asahi cells again exhibit comparable photocurrents, although they are all significantly higher than the photocurrent from the flat cell.

Comparing the shapes of the red side of the EQE curve gives further information about the observed photocurrent increases. The spectra for the flat reference cell and the Asahi reference cell are extremely smooth across the spectral range where a-Si:H is absorbing. The nanopatterned cells exhibit several peaks, which sharpen at longer wavelengths. These peaks are highly

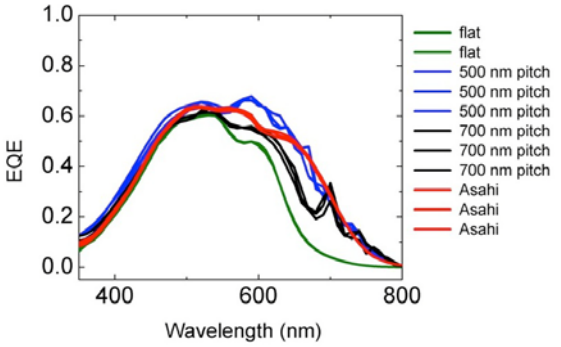

Figure 4: EQE measurements taken on multiple flat, randomly textured Asahi, and nanoimprinted cells across the substrate.

reproducible for all cells of each pitch, and are attributed to coupling to waveguide modes of the structure (see below). As the absorption of a-Si:H decreases for longer wavelengths these modes appear in more discrete bands of enhanced photocurrent.

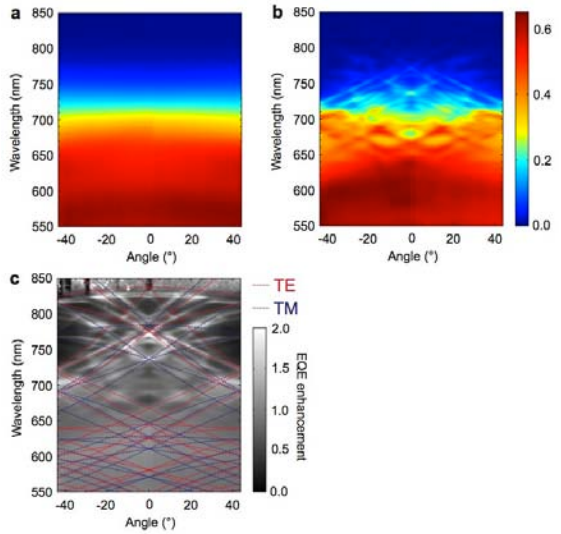

Figure 5: Measured angle-resolved EQE for 160 nm thick a-Si:H cells. (a) Asahi cell (b) 500 nm pitch cell (c) photocurrent enhancement calculated by dividing the date in panel b and panel; superimposed is a dispersion calculation of coupling to waveguides modes in the a-Si:H layer.

To investigate the nature of these modes, we measured angle-resolved external quantum efficiencies for the Asahi and nanopatterned cells, shown in Figure 5. The Asahi cell exhibits an extremely isotropic response with changing angle. Fig. 5(b) shows the 500 nm pitch cell, which shows several interesting features which sharpen at longer wavelength. The background of Fig. 5(c) shows the photocurrent enhancement, calculated by dividing the data in Fig. 5(b) and Fig. 5(a). From 550 – 650 there a broad and essentially dispersionless enhancement over the randomly textured cell is observed. From 650 – 850 nm the features become sharper and there is stronger enhancement, although only at discrete wavelengths. Overlaid on Fig. 5(c) is a dispersion diagram corresponding to coupling of normally-incident light to the waveguide modes supported by this structure, with the mode centered in the a-Si:H layer. The

calculations explain many of the crossings and broad features observed, particularly in the 650-750 nm range, indicating that the enhanced photocurrent is due to coupling to waveguide modes. From 550 – 650 nm there are many modes supported, and the absorption is very high, leading to broadening. Additionally, there are some broad features that are not well explained by the mode calculation; these may be due to localized enhancements in the vicinity of the scatterers. Weighting that data at each angle by the solar spectrum shows that the photocurrent of the nanopatterned cell exceeds that of the randomly textured cell for angles up to 25°.

5 ELECTROMAGNETIC SIMULATIONS

Finite difference time domain (FDTD) simulations were performed using Lumerical software. The layer thicknesses were taken from the experimental cross sections, and the optical constants from data measured using ellipsometry. The Ag was modeled using a Lorentz-Drude fit to Palik data [11]. For the patterned case, the nanostructures were assumed to be hemiellipsoids with diameters and geometry for each layer derived from the experimental cross sections. The unit cell was chosen to equal the pitch between scatterers, with periodic boundary conditions as drawn in Figure 6. To model the randomly textured Asahi cell, AFM scans of the bottom interface were fed directly into simulation, and the successive layers were assumed to be completely conformal with identical texture. Periodic boundary conditions were used here as well, but the unit cell was chosen to be sufficiently large to minimize any coherent effects from the periodicity.

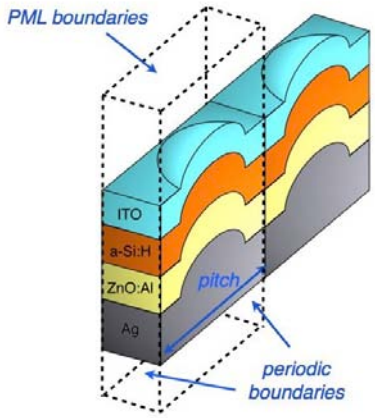

Figure 6: Schematic cross section of the a-Si:H solar cell design showing the unit cell and assumed boundary conditions for electromagnetic simulations.

The effect of doping in the *n* and *p* layers on the optical constants was neglected in the optical model, so the entire a-Si:H region is assumed to be intrinsic and optically active. The optical generation rate in the structure was calculated directly from the magnitude of the electric field **E** and the imaginary part of the permittivity for each material ε''.

$$G_{opt} = \frac{1}{2\hbar}\varepsilon''|E|^2 \qquad (1)$$

The generation rate in each material can be isolated by mapping the spatially-dependent generation rate against the refractive index. Under the assumption that all photogenerated carriers are collected, this can be converted to a photocurrent, and the calculation at each wavelength can be weighted by the solar spectrum to determine a maximum achievable J_{sc}.

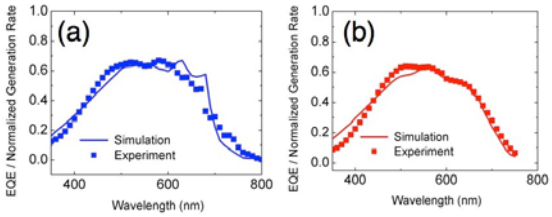

Figure 7: Comparison of measured EQE (squares) and simulated generation rate (line) for cells with 160 nm thick a-Si:H and 300 nm diameter Ag scatterers (a) and Asahi texture (b).

Figure 7(a) shows a comparison between the measured EQE of a 500 nm pitch cell with 300 nm diameter Ag scatterers and the generation rate for calculated using FDTD. Figure 7(b) shows simulation vs. experimental data for the cells made on the Asahi substrate. In both cases the overall trends as well as several of the finer features in the graphs are well reproduced. The differences between the model and experiment are likely to be due to differences in the assumed geometry and small discrepancies between measured and actual optical constants.

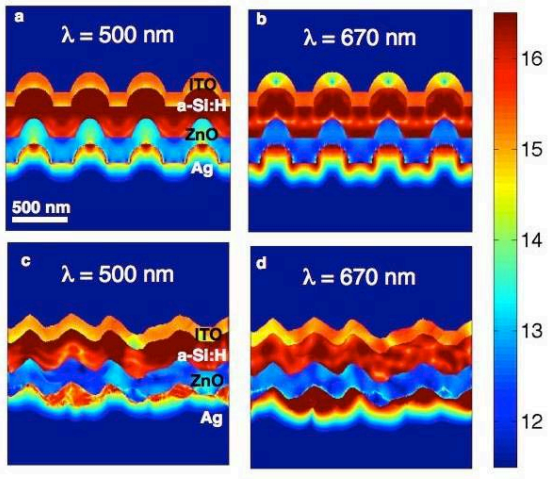

Figure 8: Generation rate maps of the simulated nanopatterned (a and b) and Asahi cells (c and d) at two different wavelengths. The color scale is logarithmic in electrons sec^{-1} cm^{-3}.

Using electromagnetic simulation cross sectional maps of the generation rate were made at specific wavelengths. Figure 8 shows generation rate maps for the 500 nm pitch nanopatterned cell and the Asahi cell at two individual simulation wavelengths, 500 nm and 670 nm. The simulations are fully three-dimensional, but only two-dimensional cross sections are shown in these images. To calculate the curves shown in Figure 7, the generation rate is integrated over only the portion containing a-Si:H, but here we show absorption in all of the layers, as it is instructive to identify the loss mechanisms.

In all four images, it is clear that the ZnO:Al layer has very low loss and that the a-Si:H is the most strongly absorbing layer. The ITO and the Ag both have significant parasitic absorption, the latter particularly for λ = 670 nm. Indeed, absorption by Ag a major loss factor for the longer wavelengths. It is also clear that the periodic structures show much more regular features of light absorption than the Asahi textured cell. For the nanopatterned cell, the main difference between the two wavelengths is the clear modal shape observed in the longer wavelength; at λ = 500 nm the absorption is almost entirely in the top portion of the cell. In the randomly textured cells, both the absorption in the a-Si:H and the parasitic absorption in the Ag tend to be concentrated around the tips of the convex portions.

6 SUMMARY AND CONCLUSION

In summary, we have demonstrated plasmonic nanopatterned ultrathin-film solar cells with photocurrents and efficiencies exceeding that of randomly textured cells. Through analysis of the EQE and angle-resolved EQE curves, we are able to identify that the photocurrent enhancement is due largely to coupling of the incoming light, scattered at the backpattern, to waveguide modes of the a-Si:H layer. Electromagnetic simulation agrees well with the experimental measurements, and we are able to use it as a tool to visualize both current-generating and parasitic absorption. Effectively, in this design sunlight is redirected in a direction orthogonal to the direction of carrier collection, enabling the use of thin semiconductor layers. Our method is applicable to all semiconductor materials that can be integrated with a nanopatterned structure. Using the imprint technique we have precise control over the fabricated patterns, which is an advantage over other techniques, such as hot sputtering of Ag, anisotropic etching of ZnO, or atmospheric pressure chemical vapor deposition of SnO_2:F [12-14] that lead to random structures with limited control over geometry. We demonstrate that thinner cells show higher open circuit voltage, due to reduced bulk recombination. Moreover, for ultrathin a-Si:H cells, an added advantage of reducing layer thickness is that this strongly reduces the photodegradation (Staebler-Wronski effect) [15]. More work is necessary to determine the best pattern design for optimal scattering. Careful engineering of the spectrum of spatial frequencies describing the patterns is required to reach an optimum light trapping design.

7 ACKNOWLEDGEMENTS

We are grateful to C. H. M. van der Werf for solar cell deposition, and to L. A. Sweatlock, I. M. Pryce, and R. de Waele for illuminating discussions. The Caltech portion of this work was supported by the Department of Energy under contract number DE-FG02-07ER46405 (modeling) and DE-FG36-08GO18006 (fabrication). Work at AMOLF is part of the research program of FOM which is financially supported by NWO. The work at Utrecht University was fully supported internally. This work is part of the Smart-Mix program Memphis and the Global Climate and Energy Project (GCEP).

8 REFERENCES

[1] H. A. Atwater and A. Polman. “Plasmonics for Improved photovoltaic devices”, Nat. Mater. 9, 2010, pp. 205-213.
[2] K. R. Catchpole, A. Polman. “Design principles for particle plasmon enhanced solar cells”, Appl. Phys. Lett. 93, 2008, 191113.
[3] F. J. Beck, A. Polman, K. R. Catchpole. “Tunable light trapping for solar cells using localized surface plasmons”, J. Appl. Phys. 105, 2009, 114310.
[4] C. F. Bohren, D. R. Huffman. Absorption and Scattering of Light by Small Particles, Wiley, 2008.
[5] B. P. Rand, P. Peumans, S. Forrest. “Long-range absorption enhancement in organic tandem thin-film solar cells containing silver nanoclusters”, J. Appl. Phys. 96, 2004, pp. 7519-7526.
[6] V. E. Ferry L. A. Sweatlock, D. Pacifici, and H. A. Atwater. “Plasmonic nanostructure design for efficient light coupling into solar cells”, Nano Lett. 8, 2008, pp.4391-4397.
[7] V.E. Ferry, M.A. Verschuuren, H.B. Li, R.E.I. Schropp, H.A. Atwater, and A. Polman. “Improved red-response in thin film a-Si:H solar cells with soft-imprinted plasmonic back reflectors”, Appl. Phys. Lett., 95, 2009, 183503.
[8] V. E. Ferry, M.A. Verschuuren, H.B.T. Li, E. Verhagen, R.J. Walters, R.E.I. Schropp, H.A. Atwater, and A. Polman, “Light trapping in ultrathin plasmonic solar cells”, Opt. Exp. 18, 2010, pp. A237-A245.
[9] K. Söderström, F.J. Haug, J. Escarré, O. Cubero, and C. Ballif, Res. Soc. Sym. Proc. 1002, 2007, pp. N03-N05.
[10] M.A. Verschuuren, Substrate Conformal Imprint Lithography for Nanophotonics, PhD Thesis, Utrecht University, The Netherlands (2010). M.A. Verschuuren, and H.A. van Sprang. “3D photonic structures by sol-gel imprint lithography”, Mater. Res. Soc. Sym. Proc. 1002, 2007, pp. N03-N05;
[11] A. D. Rakic, A.B. Djurišic, J.M. Elazar, M. Jovan, and M.L. Majewski, “Optical properties of metallic films for vertical-cavity optoelectronic devices”, Appl. Opt. 37, 1998, pp. 5271-5283.
[12] R. H. Franken, R. L. Stolk, H. Li, C. H. M. van der Werf, J. K. Rath, and R. E. I. Schropp,. “Understanding light trapping by light scattering textured back electrodes in thin film n-i-p type silicon solar cells”, J. Appl. Phys. 102, 2007, 014503.
[13] U. Dagkaldiran, et al. “Amorphous silicon solar cells made with SnO_2:F TCO films deposited by atmospheric pressure CVD”, Mater. Sci. Eng. B, 159-160, 2009, pp. 6-9.
[14] J. Krč, F. Smole, M. Topič. “Potential of light trapping microcrystalline silicon solar cells with textured substrates”, Prog. Photovolt. Res. Appl. 11, 2003, pp. 429-436.
[15] D. L. Staebler, C. R. Wronski. “Reversible conductivity changes in discharge-produced amorphous silicon”, Appl. Phys. Lett. 31, 1977, pp. 292-294.